Contribution from the Department of Chemistry,
University of Wyoming, Laramie, Wyoming 82071

Physical Properties of Linear-Chain Systems. 5. Optical Spectrum of $(CH_3)_4NMnBr_3$ (TMMB)[1]

CHARLES F. PUTNIK, G. MATTNEY COLE, and SMITH L. HOLT*

Received January 7, 1976 AIC60008R

The optical spectrum of $(CH_3)_4NMnBr_3$, TMMB, has been measured at several temperatures between ambient and 4.2 K. The transition intensities are found to be enhanced some 2–3 orders of magnitude over those observed in isolated Mn^{2+} complexes. There is spectral evidence of a phase transition near 145 K which involves a change in the Mn^{2+} microsymmetry and results in increased splitting of trigonal levels and anomalous discontinuities in the variation of oscillator strengths with temperature. Unlike the spectrum of the chloride analogue, TMMC, structure is observed on several manifolds, some of which can be attributed to phonon coupling. There is also evidence of transitions to states of appreciable doublet character, also unobserved in the spectrum of TMMC.

Introduction

The compound $(CH_3)_4NMnBr_3$, TMMB, belongs to a class of compounds which display predominantly unidimensional magnetic properties.[2] These materials are of the general formulation ABX_3 (where $A^+ = Cs^+, Rb^+, (CH_3)_4N^+$; B = divalent 3d transition metal ion; $X^- = Cl^-, Br^-, I^-$) and crystallize in a hexagonal array of infinite chains of face-sharing BX_6^{4-} octahedra. These chains, which lie parallel to the c crystallographic axis, are separated by the A cations. This separation is sufficiently large in $(CH_3)_4NMnCl_3$, TMMC, to depress the three-dimensional ordering temperature, T_N, to 0.84 K, though correlations in one dimension are observable at ~40 K.[3,5] This unique magnetic character of TMMC is mirrored in the optical spectrum. The spin selection rule ($\Delta S = 0$) is found to be relaxed,[3] a variation of oscillator strength vs. T is observed which is not of the form $f = f_0$ [1 + $\exp(-\theta/T)$], and transition probabilities are dependent upon pair states rather than single-ion states.[4] In order to determine if similar behavior is observed for TMMB we have measured the optical spectrum of this compound from 300 to 4.2 K.

Experimental Section

Preparation. Single crystals of TMMB were prepared by slow evaporation of an equimolar mixture of $MnBr_2$ and $(CH_3)_4NBr$ which was dissolved in distilled, constant-boiling, aqueous HBr.

Crystal Structure. On the basis of precession and Weissenberg photographs we have determined TMMB to be isomorphous and isostructural with TMMC belonging to space group $P6_3/m$ with cell dimensions of a = 9.44 (1) Å and c = 6.76 (2) Å.

Spectroscopic Measurements. The single crystals were mounted on aluminum rings and placed in the sample chamber of an Oxford CF-100 cryostat. The spectrum was measured at 300, 190, 150, 120, 100, 80, 55, 30, 15, and 4.2 K and controlled and measured to ±2 K using an Oxford VC-30 temperature controller. The polarized, single-crystal spectral measurements were obtained by inserting Glan-Thompson prisms in the sample and reference light paths of a Cary 14-RI recording spectrophotometer. Measurements of the σ, π, and α spectra indicated that all transitions are electric dipole in origin. Spectral bandwidth never exceeded 0.5 nm.

Results and Discussion

The absorption spectrum of TMMB at 4.2 and 150 K is shown in Figure 1. The gross features of this spectrum can be understood in terms of the octahedral ligand field states of Mn^{2+}. The assignments are shown in the figure. Table I contains a tabulation of the energies of the various maxima at 4.2 K along with the oscillator strengths. Where adjacent absorption bands are too strongly overlapped to allow the measurement of individual oscillator strengths (e.g., the $^6A_1(S) \rightarrow {}^4A_1$, $^4E(G)$ and $^6A_1(S) \rightarrow {}^4T_2(G)$ absorptions in the $E \parallel c$ polarization), the oscillator strength of the entire manifold is given. In Figures 2–4 are displayed the detailed temperature dependences of the $^6A_1(S) \rightarrow {}^4T_1(G)\parallel$, $^4T_1(G)\perp$, $^4T_2(G)\perp$, $^4T_1(P)\parallel$, and $^4T_1(P)\perp$ absorption manifolds. In Figure 5 is a plot of $f(T)/f(4.2\text{ K})$ vs. temperature for these manifolds. While the behavior of these bands varies markedly below 120 K, there is a common discontinuity between 120 and 150 K. This is accompanied by the appearance of a splitting in most of the bands. It appears that this behavior may be equated with a phase change as a discontinuity is also observed in the EPR line width at 143 K, yet no evidence of [3] ordering is observed down to 4.2 K.[5] The nature of this change is of course open to question without detailed low-temperature structural data; however, a postulation of the nature of the microenvironment of the Mn^{2+} ions will be discussed later. In Figure 1 we display the 150-K absorption spectrum of TMMB. This particular spectrum was chosen because it represents the spectrum of the material before the f vs. T anomaly occurs. Consequently one can assume that the

Table I. Absorption Energies, Oscillator Strengths, and Assignments of the Polarized Absorption Spectrum at 4.2 K

$E \parallel c$			$E \perp c$	
Oscillator strength ($f \times 10^6$)	Obsd energy, cm^{-1}	Assignments (trigonal components)	Obsd energy, cm^{-1}	Oscillator strength ($f \times 10^6$)
2.54	18 250	$^6A(S) \rightarrow {}^4E(^4T_1(G))$	18 250	6.99
	18 970	$\rightarrow {}^4A_2(^4T_1(G))$	18 970	
	21 900	$\rightarrow {}^4E(^4T_2(G))$	21 950	5.30
			22 348	
	22 550	$\rightarrow {}^4A_1(^4T_2(G))$	22 500	
	23 170	$\rightarrow {}^4E(G)$	23 163	
	23 224	$\rightarrow {}^4A_1(G)$		
6.44	23 310	$\rightarrow {}^4E + \nu_{140}$	23 210	0.117
	23 364	$\rightarrow {}^4A_1 + \nu_{140}$		
	23 452	$\rightarrow {}^4E + 2\nu_{140}$	23 452	
	23 510	$\rightarrow {}^4A_1 + 2\nu_{140}$	23 507	
	23 585	$\rightarrow {}^4E + 3\nu_{140}$	23 585	
	23 646	$\rightarrow {}^4A_1 + 3\nu_{140}$		
	26 364		26 364	
	26 455	$\rightarrow {}^4E(^4T_2(D))$	26 455	
	26 595		26 596	
	26 745		26 745	
	26 860		26 863	
	26 987	$\rightarrow {}^4A_1(^4T_2(D))$	26 991	
3.74	~27 100		~27 100	6.84
		$\rightarrow {}^4E(D)$	27 556	
	27 667	$\rightarrow {}^4E + \nu_{115}$	27 670	
	27 785	$\rightarrow {}^4E + 2\nu_{115}$	27 783	
	27 900	$\rightarrow {}^4E + 3\nu_{115}$	~27 900	
			29 394	
	29 611		29 596	
2.49	30 139	$\rightarrow {}^4T_1(P)$	30 138	1.74
	31 447		~31 500	
	32 174	$\rightarrow {}^2\Gamma$	32 185	

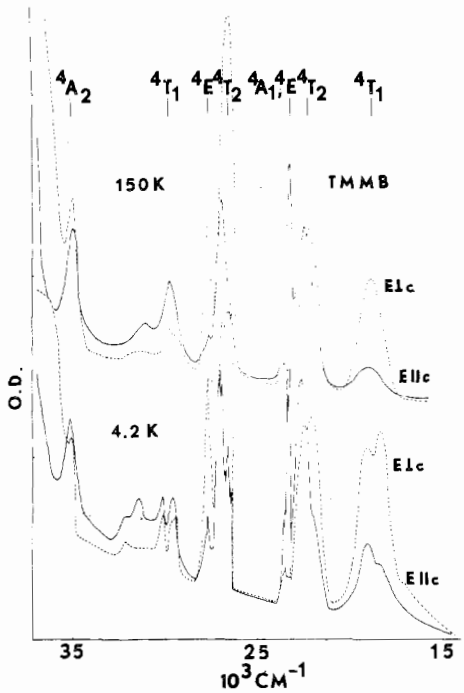

Figure 1. Polarized, single-crystal absorption spectrum of TMMB at 150 and 4.2 K. Octahedral ligand field assignment is provided and oscillator strength is in arbitrary units.

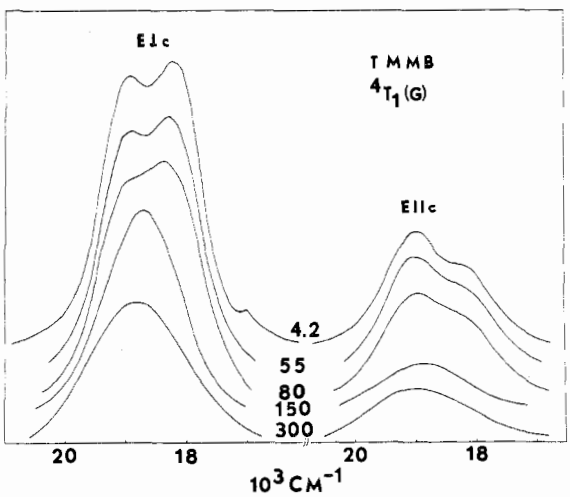

Figure 2. $E \parallel c$ and $E \perp c$ components of the $^4T_1$(G) absorption in TMMB at selected temperatures.

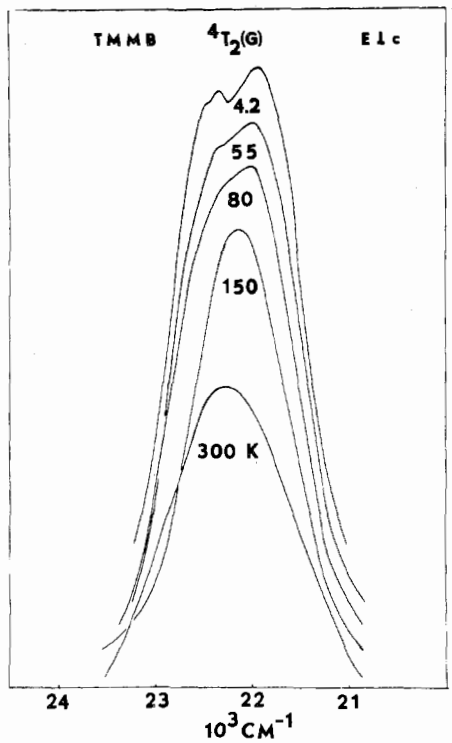

Figure 3. $E \perp c$ component of the $^4T_2$(G) absorption in TMMB at selected temperatures.

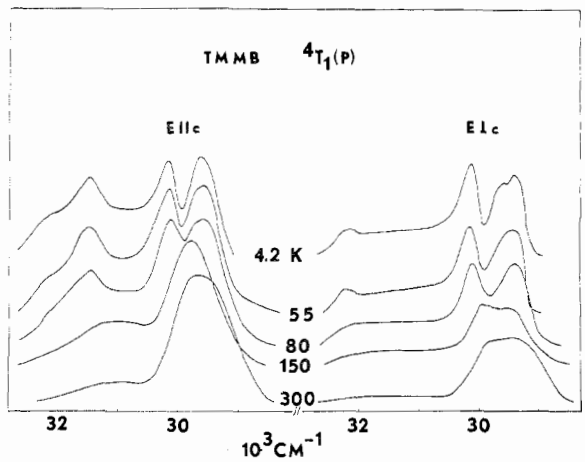

Figure 4. $E \parallel c$ and $E \perp c$ components of the $^4T_1$(P) absorption in TMMB at selected temperatures.

structure of the compound is similar to that of the room-temperature species and to that of TMMC. If we apply the results of Day and Dubicki[4] regarding the dimer transitions in TMMC (D_{3h} dimer symmetry) we expect the selection rules

$$^6A_1 \xrightarrow{\sigma} {}^4E$$

$$^6A_1 \xrightarrow{\pi} {}^4A_1$$

$$^6A_1 \nrightarrow {}^4A_2$$

It is clear from Figure 1, however, that the polarization of the lowest energy transition to the ^4E and $^4A_2$ components of $^4T_1$(G) is incomplete. Polarization of components of the $^4T_1$(P) is also incomplete. These discrepancies indicate the selection rules derived for TMMC do not fully apply to the spectrum of TMMB.

It appears instead that the mechanism operative in TMMB involves spin and orbital selection rules as moderating forces since transitions to all levels are observed though relative intensities are dependent on polarization. As stated previously the selection rules derived by Day and Dubicki[4] for the D_{3h} dimer predict transitions to $^4A_1$ states to be allowed with $E \parallel c$ and transitions to quartet levels of E symmetry to be allowed with $E \perp c$. Application of D_{3d} single-ion site symmetry selection rules predicts transitions to $^4A_2$ levels allowed with $E \parallel c$ and transitions to ^4E levels allowed with $E \perp c$. The introduction of a trigonal field causes octahedral T_1 states to split into A_2 and E components and splits T_2 states into A_1 and E components. Therefore, depending upon which scheme is employed, transitions to ^4E states are expected to be allowed with $E \perp c$ and transitions to $^4A_1$ or $^4A_2$ states allowed with $E \parallel c$. On the basis of these considerations we assign those transitions which are most intense with $E \parallel c$ as the respective A trigonal component (of T) and those most intense with $E \perp c$ as the E trigonal component.

Above 150 K there appears to be an $\sim$200-cm^{-1} splitting of the respective ^4A and ^4E trigonal components of the octahedral ^4T states. This is apparent from the differences in

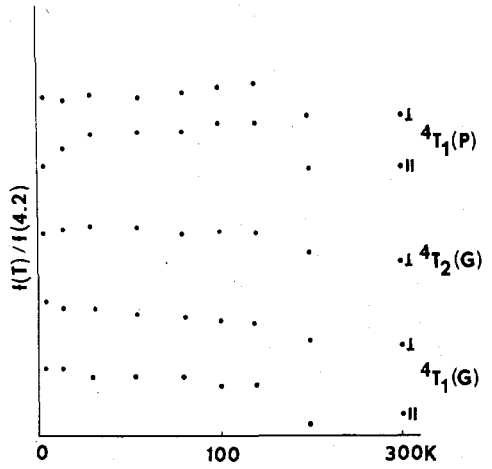

Figure 5. Temperature dependence of the oscillator strengths of selected absorptions in the spectrum of TMMB. Values for a particular band are normalized to the value at 4.2 K. Thus all 4.2-K values are equal to 1 and are separated for clarity.

energy of the absorption maxima in different polarizations. Thermal broadening causes extensive overlap of the trigonal-state absorptions and the two distinct maxima are not resolvable.

Below 150 K, the apparent phase transition appears to involve an increase in the trigonal field strength. This causes the splitting of the trigonal components of the octahedral ^4T levels to increase to $\sim$900 cm^{-1}. This separation is sufficiently large that the maxima of the individual ^4A and ^4E trigonal components are observable. The trigonal states thus observed are consistently polarized in the opposite sense and assignments are made on this basis.

We should point out that the apparent phase transition observed in this study does not appear to be analogous to the phase transition in TMMC.[7,8] The transition in TMMC involves the structural ordering of the $(CH_3)_4N^+$ groups which results in a change in space group symmetry from hexagonal to monoclinic. This change does not alter the -Mn-Cl_3-Mn- chain and is not observable in the EPR spectrum nor, it appears, in the optical spectrum.[4] The anomaly observed in TMMB, on the other hand, appears to significantly alter the microenvironment of the Mn^{2+} ions in the chain.

While the aforementioned phenomena are common to all electronic transitions in TMMB, we will discuss each manifold independently as there are distinct physical differences.

$^6A_1(S) \rightarrow {}^4T_1(G)$. At room temperature this transition exhibits an intense maximum in the $E \perp c$ direction at 18 825 cm^{-1} (^4E) and a less intense maximum at $\sim$19 000 cm^{-1} with $E \parallel c$ ($^4A_2$). Below 150 K this manifold exhibits maxima at 18 250 and 18 970 cm^{-1} in both polarizations. The maximum at 18 250 cm^{-1} is most intense with $E \perp c$ and the maximum at 18 970 cm^{-1} most intense when $E \parallel c$, Figure 2.

In both polarizations the absorption manifolds exhibit a large increase in oscillator strength between room temperature and 4.2 K with the major portion of the increase occurring between 150 and 120 K, Figure 5. Behavior of this type is generally associated with electronic transitions which are magnon/cold band assisted and derive from an exchange-induced electric dipole transition operator. The abrupt increase observed between 150 and 120 K associated with the apparent phase change can be reasonably explained by considering the phase change to alter the structure and improve exchange pathways thereby increasing the magnitude of the exchange-induced dipole moment.

$^6A_1(S) \rightarrow {}^4T_2(G)$. This manifold is overlapped in both polarizations with the $^6A_1 \rightarrow {}^4A_1$, $^4E(G)$ transition. In the $E \perp c$ polarization this overlap is sufficiently small to allow a determination of f vs. T for the manifold. Between ambient temperature and 150 K there is a slight increase in oscillator strength followed by a large discontinuous increase between 150 and 120 K. Below 120 K the oscillator strength appears to increase slightly to 30 K and then decrease slightly to 4.2 K although it does not vary markedly. In the $E \parallel c$ direction the considerable overlap with the adjacent $^6A_1(S) \rightarrow {}^4A_1$, ^4E absorption precludes the determination of oscillator strength as a function of temperature. It does appear, however, that there is a major increase in intensity from 150 to 4.2 K, Figure 6.

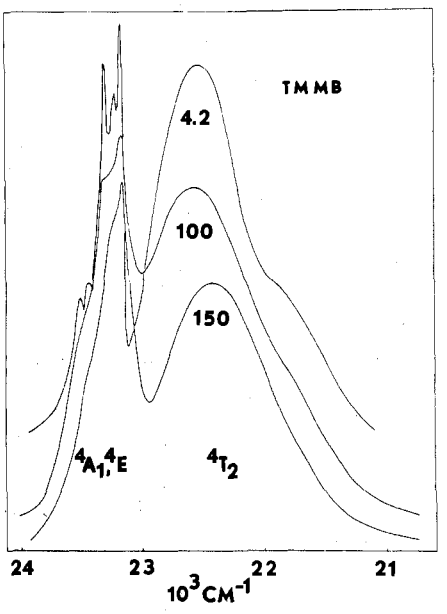

Figure 6. $E \parallel c$ components of the $^4T_2(G)$ and $^4A_1$, $^4E(G)$ absorption in TMMB at several temperatures.

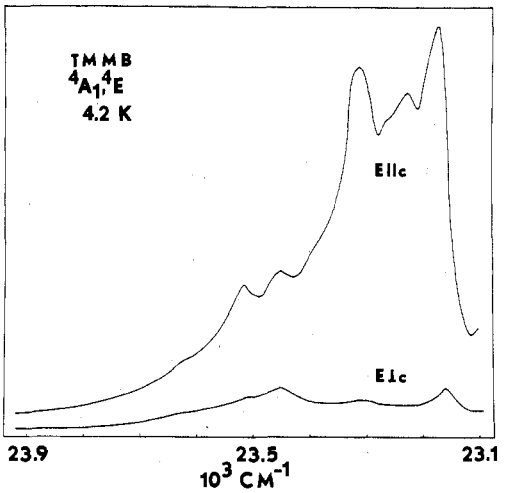

Figure 7. $E \parallel c$ and $E \perp c$ components of the $^4A_1$, $^4E(G)$ absorption in TMMB at 4.2 K.

At room temperature this manifold exhibits intense maxima at 22 422 cm^{-1} with $E \parallel c$ and 22 143 cm^{-1} with $E \perp c$. Below 150 K the absorptions in both polarizations increase in oscillator strength and take on an asymmetric character. Two distinct maxima are resolved below 55 K in both orientations. At 4.2 K with $E \parallel c$ the absorption appears as a weak shoulder near 21 900 cm^{-1} and an intense maximum at 22 550 cm^{-1}. With $E \perp c$ the manifold shows an intense maximum at 21 950 cm^{-1}, a less intense maximum at 22 348 cm^{-1}, and a shoulder near 22 500 cm^{-1}. For the reasons discussed previously we assign the absorption near 21 900 cm^{-1} to the ^4E component of $^4T_2(G)$ and the absorption near 22 500 cm^{-1} to the $^4A_1$ component of $^4T_2(G)$.

$^6A_1(S) \rightarrow {}^4A_1$, $^4E(G)$. This manifold occurs in the 23 000–24 000-cm^{-1} region and exhibits considerably more fine structure than observed in TMMC,[3,4] Figure 7. In the $E \parallel c$ orientation at 4.2 K this absorption appears as three, strong, intense, relatively sharp absorptions at 23 170, 23 224, and 23 310 cm^{-1} followed by a series of weak shoulders at 23 364, 23 452, 23 510, 23 585, and 23 646 cm^{-1}. In the $E \perp c$ orientation the manifold exhibits weak maxima at 23 163, 23 310 and 23 452 cm^{-1} and two very weak shoulders at 23 507 and 23 585 cm^{-1}. In the $E \parallel c$ polarization the maxima at 23 170, 23 310, 23 452, and 23 585 cm^{-1} appear to be components of an ~140-cm^{-1} progression as do the corresponding bands in the $E \perp c$ polarization. In addition, the $E \parallel c$ maxima at 23 224, 23 364, 23 510, and 23 646 cm^{-1} also appear to be members of a 140-cm^{-1} progression. Thus the maxima at 23 170 and 23 224 cm^{-1} are the apparent origins of individual electronic absorptions. Because the progression based on the 23 170-cm^{-1} origin is present in both polarizations, we assign it to the $^6A_1(S) \rightarrow {}^4E(G)$ transition. The other progression observed with $E \parallel c$ based on the 23 224-cm^{-1} origin is not observed with $E \perp c$ and is assigned to the $^6A_1(S) \rightarrow {}^4A_1(G)$ transition.

We must point out that this assignment is not consistent with that offered for TMMC.[4] In that work the 23 000–23 400-cm^{-1} region was attributed to the $^6A_1 \rightarrow {}^4A_1$ absorption and the 23 400–23 800-cm^{-1} region was attributed to $^6A_1 \rightarrow {}^4E$. While our assigned progressions do not show classic, phonon-assisted band shape, it is impossible to determine the effect of the strong overlap of the two progressions as well as the overlap with the $^4T_2(G)$ absorption tail on the appearance of this manifold. We also consider the observed spacings to be too consistent to be explained as a chance spacing between components of adjacent absorptions. Our result also agrees with the findings of Ferguson et al.,[6] who have found the ^4E origin at lower energy than the $^4A_1$ origin in the spectrum of Mn^{2+} in $KMgF_3$ and $KZnF_3$.

$^6A_1(S) \rightarrow {}^4T_2(D)$. At room temperature this manifold exhibits strong maxima at 26 617 cm^{-1} with $E \perp c$ and at 26 954 cm^{-1} with $E \parallel c$. It is overlapped strongly on the high-energy side with the adjacent $^6A_1 \rightarrow {}^4E(D)$ absorption in both polarizations precluding accurate determination of oscillator strength. Qualitatively the manifold increases slightly in oscillator strength between ambient temperature and 150 K. Just below 150 K the band top broadens in the $E \perp c$ orientation and a shoulder to low energy is resolved with $E \parallel c$. This is accompanied by a discontinuous decrease in the oscillator strength of the $E \perp c$ component and a discontinuous increase in the oscillator strength of the $E \parallel c$ component. As the temperature is lowered, further structure is resolved in both polarizations and the oscillator strengths of both remain fairly constant.

At 4.2 K the $E \perp c$ absorption exhibits strongly overlapped maxima at 26 364, 26 455, 26 595, 26 745, 26 860, and 26 987 cm^{-1} followed by a shoulder at ~27 100 cm^{-1}. The $E \parallel c$ absorption exhibits overlapped maxima at 26 364, 26 455, 26 596, and 26 745 cm^{-1} followed by more intense maxima at 26 863 and 26 991 cm^{-1} and a shoulder at ~27 100 cm^{-1}. Clearly, the same components are observed in each polarization. The intensities of all components are approximately equal with $E \perp c$ but the four lowest energy maxima are much less intense with $E \parallel c$. We assign the components at 26 364, 26 455, 26 595, and 26 745 cm^{-1} to the $^6A_1(S) \rightarrow {}^4E({}^4T_2(D))$ transition and the remaining higher energy maxima to the $^6A_1(S) \rightarrow {}^4A_1({}^4T_2(D))$ transition.

The spacing of the observed maxima suggests the possibility of a phonon progression or spin–orbit splitting; however, due to the ill-resolved nature of the individual components we withhold any further speculation.

$^6A_1(S) \rightarrow {}^4E(D)$. At room temperature this absorption shows a strong maximum at ~27 700 cm^{-1} with $E \perp c$ and a weak maximum at the same energy with $E \parallel c$. The absorption in both polarizations appears to increase in intensity as temperature is decreased, but the overlap with the adjacent $^6A_1 \rightarrow {}^4T_2(D)$ absorption makes quantitative measurement inaccurate. At 4.2 K the $E \perp c$ manifold appears as a weak shoulder at 27 556 cm^{-1}, an intense peak at 27 670 cm^{-1}, a well-resolved shoulder at 27 783 cm^{-1}, and a weak shoulder at ~27 900 cm^{-1}. The three $E \parallel c$ components resolved are much weaker than the $E \perp c$ counterparts. The most intense is the peak at 27 667 cm^{-1} followed by successively weaker shoulders at 27 785 and ~27 900 cm^{-1}. The spacing between maxima is ~115 cm^{-1} in both polarizations and the peaks must correspond to a phonon progression of this energy. The apparent origin with $E \perp c$ is 27 556 cm^{-1}. This peak is not observed with $E \parallel c$, and since, as discussed earlier, transitions to ^4E states are allowed with $E \perp c$, we assign this as the $^6A_1(S) \rightarrow {}^4E(D)$ origin and attribute the maxima observed with $E \parallel c$ as the components of the phonon progression minus the apparent $0 \rightarrow 0$ origin.

$^6A_1(S) \rightarrow {}^4T_1(P)$. This absorption is observed between 28 000 and 33 000 cm^{-1}, Figure 4. At room temperature with $E \parallel c$ a maximum is observed at 29 774 cm^{-1} followed by a broad, very weak maximum at ~31 000 cm^{-1}. With $E \perp c$ a broad manifold exhibiting maxima at ~29 500 and 29 940 cm^{-1} followed by a very broad and weak absorption centered near 31 300 cm^{-1} is observed. Below 150 K there is a dramatic change in the appearance of this absorption in both polarizations manifested as a splitting of both room-temperature components. As the temperature is lowered to 4.2 K the $E \parallel c$ absorption resolves into maxima at 29 611 and 30 139 cm^{-1} followed by a less intense peak at 31 447 cm^{-1} and a shoulder at 32 174 cm^{-1}. The temperature dependence of the oscillator strength indicates the possible contribution of a magnon/hot band type mechanism, Figure 5, though no side bands are resolved. The $E \perp c$ absorption exhibits maxima at 29 394, 29 596, and 30 138 cm^{-1} followed by a broad, very weak absorption centered near 31 500 cm^{-1} and a weak peak at 32 185 cm^{-1}.

The absorptions near 29 600 and 31 450 cm^{-1} are more intense with $E \parallel c$ while with $E \perp c$ the maxima at 30 140 and 32 180 cm^{-1} are more intense. In addition the perpendicular absorption at ~29 500 cm^{-1} is resolved into two components at 29 394 and 29 596 cm^{-1} below 55 K. By the polarization criteria discussed earlier we would assign the absorptions at 29 500 and 31 450 cm^{-1} to transitions to $^4A_2$ trigonal states and those at 30 140 and 32 180 cm^{-1} to transitions to ^4E states. This assignment is not realistic if the transitions all involve levels deriving from $^4T_1(P)$. The apparent room-temperature splitting of ~1500 cm^{-1} is also anomalously large when compared to the ~300-cm^{-1} separation measured in the other manifolds. A reasonable explanation derives from the recent work of Ferguson et al.[6] which indicates that spin–orbit components of a doublet level interact strongly with the $^4T_1(P)$ components from higher energy. The absorptions at 31 450 and 32 180 cm^{-1} may then be attributed to transitions to levels of appreciable doublet character.

While this explains the number of absorptions, we are left to explain a "splitting" in a level of apparent A_2 symmetry in the $E \perp c$ orientation near 29 500 cm^{-1}, Figure 4. This appears to be a splitting in the transition between an orbitally nondegenerate ground state ($^6A_1$) and an orbitally nondegenerate excited state ($^4A_2$). However, referring again to the results of Ferguson et al.,[6] the four octahedral, spin–orbit components of $^4T_1(P)$ are separated by ~200 cm^{-1} and the imposition of a trigonal field would split the octahedral states

into six trigonal components. It appears, then, that the absorption manifold observed between 28 000 and 33 000 cm^{-1} results from transitions to spin–orbit components of $^4T_1(P)$ and those of a doublet level which interact strongly with these.

Summary and Conclusions

When viewed in total, this work has measured oscillator strengths of spin-forbidden $^6A_1 \rightarrow {}^4\Gamma$ transitions in TMMB which are enhanced 2–3 orders of magnitude over those of isolated Mn^{2+} complexes. The apparent observation of transitions to states of substantial doublet character indicates the operative mechanism of enhancement is not limited to $\Delta S = 1$ transitions and, since this is not observed in TMMC, implicates the bridging bromide ligands as important contributors. The observed anomalies in oscillator strengths as functions of temperature and the increased splitting of measured components all near 150 K indicate a phase transition in TMMB which is not analogous to the phase transition in TMMC[7,8] and suggest a need for low-temperature structural information to more fully understand the phenomenon.

Acknowledgment. The authors wish to thank Dr. B. B. Garrett for many useful discussions of this work. This research was supported by National Science Foundation Grant No. GP-41056 and by the Office of Naval Research.

Registry No. TMMB, 51139-56-1.

References and Notes

(1) Part 4: C. F. Putnik, G. M. Cole, and S. L. Holt, *Inorg. Chem.*, **15**, 2001 (1976).
(2) J. Ackerman, G. M. Cole, Jr., and S. L. Holt, *Inorg. Chim. Acta*, **8**, 323 (1974).
(3) R. Dingle, M. E. Lines, and S. L. Holt, *Phys. Rev.*, **187**, 643 (1969).
(4) P. Day and L. Dubicki, *J. Chem. Soc., Faraday Trans. 2*, **69**, 363 (1973).
(5) B. B. Garrett, C. F. Putnik, S. Buskirk, and S. L. Holt, to be submitted for publication.
(6) J. Ferguson, H. U. Güdel, E. R. Krauz, and H. J. Guggenheim, *Mol. Phys.*, **28**, 879 (1974).
(7) B. W. Mangum and D. B. Utton, *Phys. Rev. B*, **6**, 2790 (1972).
(8) P. S. Purcy and B. Morosin, *Phys. Lett. A*, **36**, 409 (1971).

Contribution No. 2860 from the Department of Chemistry, Indiana University, Bloomington, Indiana 47401

Reactions of MCl_6^{2-} (M = Ti, Mo, W) with $CrCl_2$ and Cl^- in CH_2Cl_2

M. S. MATSON and R. A. D. WENTWORTH*

Received February 17, 1976 AIC601232

The reactions of $[(n\text{-}C_4H_9)_4N]_2MCl_6$ (M = Ti, Mo, W) with equimolar quantities of $CrCl_2$ and $[(n\text{-}C_4H_9)_4N]Cl$ in CH_2Cl_2 have been examined. When M = Mo, the smooth reaction in the absence of air produces the anion $CrMoCl_9^{3-}$ which does not dissociate into $Cr_2Cl_9^{3-}$ and $Mo_2Cl_9^{3-}$. The reaction of this substance with either dry air or O_2 produces $CrMoOCl_9^{3-}$. No reaction occurs when M = W. When M = Ti, an equilibrium mixture of $Ti_2Cl_9^{3-}$, $Cr_2Cl_9^{3-}$, and $TiCrCl_9^{3-}$ is obtained. Additional studies have indicated that $Cr_3Cl_{10}^{4-}$ is formed when $CrCl_2$ dissolves in CH_2Cl_2 which contains an equimolar quantity of $[(n\text{-}C_4H_9)_4N]Cl$. The formation of $CrCl_4^{2-}$ appears to occur upon the addition of more alkylammonium chloride.

Introduction

Although there are increasing numbers of metal cluster compounds, their syntheses have been discovered generally by chance. One of the long-range goals of this laboratory has been the development of rational syntheses for the confacial, bioctahedral anions $M_2Cl_9^{3-}$. Our first effort, which was directed toward the synthesis of $W_2Cl_9^{3-}$, ended in failure.[1] However, more recent investigations[2,3] led to the designed synthesis of $Mo_2Cl_9^{3-}$, as well as a new anion, $Mo_3Cl_{12}^{3-}$. Another long-range goal was to develop extensions of these methods such that anions containing two different metal atoms, $MM'Cl_9^{3-}$, could be synthesized. Any synthetic system which seemed to rely principally upon entropy to achieve the desired goal was not considered. Thus, there was no attempt to achieve success by the route

$$M_2Cl_9^{3-} + M'_2Cl_9^{3-} \rightleftharpoons 2MM'Cl_9^{3-}$$

However, the synthesis of $CrMoCl_9^{3-}$, according to reaction 1 in CH_2Cl_2, as well as the logic behind that synthesis, has

$$MoCl_6^{2-} + CrCl_2 + Cl^- \rightarrow CrMoCl_9^{3-} \quad (1)$$

been presented in a previous communication.[4] Crucial, irrefutable evidence showed that the product was not an equimolar mixture of $Cr_2Cl_9^{3-}$ and $Mo_2Cl_9^{3-}$.

Further details about reaction 1 and the characterization of $CrMoCl_9^{3-}$ and its oxidation product need to be discussed. The successful isolation and characterization of this anion prompted attempts to prepare $CrWCl_9^{3-}$ and $TiCrCl_9^{3-}$ through corresponding reactions using WCl_6^{2-} and $TiCl_6^{2-}$, respectively. Details about these reactions and their products will be discussed. Finally, the nature of $CrCl_2$ and Cl^- in CH_2Cl_2 will be explored.

Experimental Section

Reagents and Procedures. Samples of $[(n\text{-}C_4H_9)_4N]Cl$ were dried at 45 °C over P_2O_5 under a dynamic vacuum for 15–24 h. Argon was purified by passing it successively through heated copper turnings and P_2O_5. The solvents were dried and distilled before placing in storage flasks on the vacuum line. Solutions of $[(n\text{-}C_4H_9)_4N]Mo(CO)_4Cl_3$ were prepared by a procedure similar to that of Bowden and Colton[5] which involves the chlorination of known quantities of $Mo(CO)_6$ at −80 °C in a container sealed by a stopcock. Gases were then removed under vacuum before the addition of stoichiometric quantity of $[(n\text{-}C_4H_9)_4N]Cl$ in CH_2Cl_2 at −80 °C. The synthesis of $[(n\text{-}C_4H_9)_4N]_2TiCl_6$ was accomplished by the reaction of stoichiometric quantities of distilled $TiCl_4$ and the alkylammonium halide in CH_2Cl_2, followed by precipitation with ether. The preparation of $[n\text{-}C_4H_9)_4N]_2MoCl_6$ was accomplished by a new method from $Mo(CO)_6$, $[(n\text{-}C_4H_9)_4N]Cl$ (1:2 mole ratio), and excess Cl_2 in CH_2Cl_2 at room temperature. Anal. Calcd: Cl, 26.8. Found: Cl, 26.7. Similar procedures with $W(CO)_6$ afforded $[(n\text{-}C_4H_9)_4N]WCl_6$. Reduction to $[(n\text{-}C_4H_9)_4N]_2WCl_6$ was accomplished with Sn powder suspended in CH_2Cl_2 in the presence of a stoichiometric quantity of $[(n\text{-}C_4H_9)_4N]Cl$. The electronic and infrared spectra were identical with those which were published earlier.[1] Samples of the $[(n\text{-}C_4H_9)_4N]^+$ salts of $Cr_2Cl_9^{3-}$ and $Mo_2Cl_9^{3-}$ were obtained from published procedures,[3,6] but the yield of the latter was increased to 95%. Two methods were used for the preparation of $[(n\text{-}C_4H_9)_4N]_3Ti_2Cl_9$: the combination of stoichiometric quantities of $TiCl_3$ and $[(n\text{-}C_4H_9)_4N]Cl$ in CH_2Cl_2 or the reduction of $TiCl_4$ with Sn powder in CH_2Cl_2 in the presence of stoichiometric quantities of